Gold Superfill in Submicrometer Trenches: Experiment and Prediction

D. Josell,[z] D. Wheeler, and T. P. Moffat*

National Institute of Standards and Technology, Metallurgy Division, Gaithersburg, Maryland 20899-8554, USA

Bottom-up deposition of gold in fine trenches, also called "superfill," was recently demonstrated using a submonolayer coverage of preadsorbed, deposition-rate-accelerating lead followed by gold electrodeposition. The present study has used experiments on planar substrates to quantify the effect of Pb adsorption on the Au deposition rate and the rate at which the adsorbed Pb was consumed during the Au deposition process. The values obtained have been incorporated into the curvature enhanced accelerator coverage mechanism of superfill where they were used to quantitatively predict the nonconformal, bottom-up deposition observed during filling of the patterned features. The results indicate the potential of the process for damascene interconnect fabrication in GaAs, GaN, and related technologies.
© 2005 The Electrochemical Society. [DOI: 10.1149/1.2128765] All rights reserved.

The bottom-up "superfill" process for fabrication of copper interconnects[1] is now the standard for state-of-the-art interconnect fabrication within the silicon-based semiconductor industry. However, gold is used to form a variety of ohmic and Schottky contacts for semiconductor technologies based on, for example, gallium arsenide[2] and gallium nitride[3] as well as for chip-level wire bonding; hence, an interest exists in a process for fabricating gold interconnects. A bottom-up, "superfill" process for Au that would be appropriate for fabricating interconnects in damascene processing was recently demonstrated for Au superfill in fine trenches,[4] as was an alternative process.[5] The present paper uses measurement techniques and models first developed to understand the related copper superfill process in order to elucidate the relevant kinetics of the new Au superfill process. The kinetics obtained are then used to quantitatively predict the Au superfill process.

While several mechanisms have been proposed to underlie the superfill process during electrochemical deposition (ECD) of copper,[6-9] the curvature-enhanced accelerator coverage (CEAC) mechanism[8,9] has been demonstrated to quantitatively predict superfill during electrodeposition of copper[8-12] and silver[13-16] and chemical vapor deposition of copper.[17] The CEAC mechanism predicts that an electrolyte-additive system can yield superfill when two requirements are met: (*i*) the additive adsorbs on the deposit surface and accelerates the local deposition rate and (*ii*) the adsorbed additive remains on the surface of the deposit during deposition. Under these circumstances, the CEAC predicts that the decreasing area of the metal surface at the bottoms of filling features will lead to locally increasing coverage of the adsorbed accelerator, which will lead to increased local deposition rate and bottom-up superfill. Predictive models based on the CEAC mechanism use kinetics obtained from studies on planar substrates; no additional parameters are needed for simulating feature filling or more general interface evolution. Because superfill processes based on the CEAC mechanism derive from surface segregation of adsorbates, they not only eliminate void and seam formation but might also be expected to yield high-purity, high-conductivity deposits needed for semiconductor interconnects.

Acceleration of the Au deposition rate from $KAu(CN)_2$ in the presence of a surfactant adsorbate, the key to feature superfill according to the CEAC mechanism, has been detailed for a variety of additive-containing electrolytes;[18-25] these include studies of accelerated Au deposition in the presence of adsorbed Pb.[22,24] The acceleration is presumed to arise from the impact of the adsorbate on the rate-limiting step in kinetically controlled Au deposition from $KAu(CN)_2$. A variety of mechanisms and rate-limiting steps have

been proposed, all involving an adsorbed intermediate AuCN or $AuCN^-$ layer.[22,26,27] Such an adsorbed cyanide intermediate has been viewed directly[28] by scanning tunneling microscopy as well as by vibrational spectroscopy.[29]

Like Pb, adsorbed Tl also increases the Au deposition rate, making related research potentially relevant. In particular, the decreased coverage of CN-containing species on the Au surface in the presence of adsorbed Tl has been detailed.[25] It has also been seen that the use of Tl additive decreases the hardness and lowers the impurity content of Au deposits.[30] The impact of Tl adsorbate on the Au deposition rate[31] has been noted to increase with temperature.

It was on the basis of the CEAC mechanism that the electrolyte-additive system was selected for the first Au superfill study.[4] That work, while disclosing a process for Au superfill, did not obtain the kinetic parameters required for CEAC-based prediction of the process itself. As such it was unable to provide quantitative comparison of theory and experiment. This work attempts to do both.

General Experimental Details

The experiments detailed in this work utilized the same electrolyte (0.02 mol/L $KAu(CN)_2$, 0.1 mol/L KOH, and 0.1 mol/L KCN in 18 MΩ water) and $Pb(NO_3)_2$ additive used in the first Au superfill process.[4] Electrolytes were used in 100-mL quantities that were sparged with nitrogen or argon immediately prior to use in order to remove oxygen that otherwise contributes a Pb coverage-dependent current density that interferes with interpretation of current measurements in terms of Au deposition rate.[32] All depositions were conducted at room temperature (~23°C) under flowing nitrogen or argon, and the platinum counter electrode was placed on the opposite side of the beaker from the specimen.

Studies of kinetics were conducted on Si wafers coated with 80-nm Au using a 10-nm Ti, 10-nm Pd adhesion layer, in order from the substrate, all deposited by electron-beam evaporation. The specimens were masked with plater's tape to expose a circular area of 0.98 cm². Studies of superfill in trenches were conducted on patterned wafers with bilayer seeds of 3-nm Ti and 27-nm Au. Deposit thicknesses on the sidewalls of the trenches were approximately one-tenth these values.

Formalism of the CEAC Mechanism

Quantitative modeling of superfill through the CEAC mechanism requires establishing the forms and parameters of two principal equations. The first equation quantifies the relationship between adsorbate coverage and metal deposition rate (i.e., current density). The second equation quantifies the evolution of the adsorbate coverage. These two equations, with boundary conditions based on physical understanding of conservation of metal and adsorbate at the interface and transport within the electrolyte, allow for quantitative prediction of feature filling.

* Electrochemical Society Active Member.
[z] E-mail: daniel.josell@nist.gov

Table I. Constants with kinetic parameters from fitting of current transients on planar substrates as used to model filling of patterned specimens.

F, C/mol	96,485
i_L, mA/cm^2	1.2
$i^{\theta=0}$, mA/cm^2	0.048
$i^{\theta=1}$, mA/cm^2	1.04
k_+, cm^3/mol s	1×10^6
k_-, 1/cm	2.8×10^4
Ω, cm^3/mol	10.21
δ, cm (stagnant)	0.027
δ, cm (agitated)	0.009
Γ, mol/cm^2	7×10^{-10}
C^o_{Au}, mol/cm^3	2×10^{-5}
$\left. \dfrac{di}{dt} \right|_{drift}$, mA/cm^2 s	6×10^{-5}
D_{Au}, cm^2/s	1.7×10^{-5}
D_{Pb}, cm^2/s	1.7×10^{-5}

The equation quantifying the relationship between the adsorbate coverage and the local deposition rate is obtained from the product of the concentration of Au ions in the electrolyte adjacent to the interface, C^i_{Au}, and a linear combination of the electrochemical rate constants for deposition on Au- and Pb-catalyzed surfaces, k_{Au} and k_{AuPb}, weighted by the respective surface coverage of each in this two-state system. In terms of the fractional Pb adsorbate coverage, θ_{Pb}, this is written

$$i(\theta_{Pb}) = F \frac{C^i_{Au}}{C^o_{Au}} [k_{Au}(1 - \theta_{Pb}) + k_{AuPb}\theta_{Pb}] \quad [1]$$

For psuedo-steady-state transport across a boundary layer, the Au-ion concentration at the surface of the planar deposit can be expressed in terms of the current by

$$\frac{C^i_{Au}}{C^o_{Au}} = \left(1 - \frac{i(\theta)}{i_L}\right) \quad [2]$$

where i_L is the transport-limited current (obtained from cyclic voltammetry, not shown, and given in Table I). Also, θ has been used in place of the more explicit θ_{Pb}, as it is henceforth. The rate constants for deposition are given by

$$k_i = k_i^o \exp\left(-\frac{\alpha_i F \eta}{RT}\right) \quad [3]$$

Because the analyzed measurements were taken at constant overpotential η and lacking information to the contrary, the transfer coefficients α_i have been presumed independent of the nature of the surface, i.e., $\alpha_{Au} = \alpha_{AuPb}$ [$\eta = -0.14$ V as all experiments were conducted at -0.95 V vs a saturated calumel reference electrode (SCE) with cyclic voltammetry, not shown, indicating -0.81 V SCE as the equilibrium potential for reversible Au deposition/dissolution]. With this assumption, Eq. 1 can be rewritten in terms of the partial currents for a Au surface ($\theta = 0$) and a Pb-saturated surface ($\theta = 1$) to give

$$i(\theta) = \frac{C^i_{Au}}{C^o_{Au}}[(1 - \theta)i^{\theta=0} + \theta i^{\theta=1}] = \left(1 - \frac{i(\theta)}{i_L}\right)[(1 - \theta)i^{\theta=0} + \theta i^{\theta=1}] \quad [4]$$

Equation 4 can be rewritten to express the current density i as a function of the adsorbate coverage θ

$$i(\theta) = \frac{i^*(\theta)}{1 + \frac{i^*(\theta)}{i_L}} \quad [5]$$

where, for convenience, the shorthand $i^*(\theta) \equiv (1 - \theta)i^{\theta=0} + \theta i^{\theta=1}$ has been defined.

For this study, the equation describing the evolution of adsorbate coverage through area change, accumulation from the electrolyte and consumption through incorporation in the deposit was written

$$\frac{d\theta}{dt} = \theta\kappa\frac{\Omega_{Au}}{F}i(\theta) + k_+C^i_{Pb}(1 - \theta) - k_-\theta\frac{\Omega_{Au}}{F}i(\theta) \quad [6]$$

The first term, which imposes mass conservation during area change on the moving interface, gives the CEAC mechanism its name. It expresses the normalized rate of area change in terms of the local curvature κ and the normal velocity v (where v equals the product of the molar volume Ω_{Au} and current density i divided by Faraday's constant F for the monovalent Au ion in the electrolyte). It is this term, which accounts for compression or dilation of the adsorbate coverage during deposition on nonplanar surfaces ($\kappa \neq 0$), that underlies the superfill phenomenon. The second term assumes Langmuir adsorption kinetics to give accumulation occurring at a rate proportional to the concentration C^i_{Pb} of Pb in the adjacent electrolyte and the fraction of available sites on the surface of the deposit (rate constant k_+). The third term invokes the loss, presumed in this work to be through burial, of a constant fraction of adsorbate during each increment of growth; it can be found in a previously published model of adsorbate consumption for modeling of leveling.[53] Recalling the relationship between the growth velocity v and current density i, the constant k_- in Eq. 6 can be shown to be the fraction of adsorbates that are buried per unit increase of deposit thickness.

Kinetics for Eq. 5 and 6 were obtained from the results of two different types of experiments on planar substrates. The next section details these experiments.

Studies of Kinetics on Planar Substrates

Current increase during accumulation.— The first type of experiment involved concurrent Pb adsorption and Au electrodeposition from Au-cyanide electrolytes containing different Pb(NO$_3$)$_2$ concentrations. These experiments were conducted at -0.95 V SCE without agitation. They yielded rising current–time transients associated with the gradual, concentration-dependent accumulation of the rate-accelerating Pb adsorbate (see Fig. 1).

Current decay after derivatization.— The second type of experiment began with simultaneous Pb accumulation/Au deposition as described in the preceeding section, though for short, controlled periods, that was followed by transfer of the specimen to Pb-free electrolyte for a longer period of Au deposition, again at -0.95 V SCE without agitation. For most of these experiments, the Au-cyanide electrolyte used for the first step had a 10 μmol/L concentration of the Pb(NO$_3$)$_2$ additive, although some of the accumulation steps were done with 8 μmol/L Pb(NO$_3$)$_2$ concentrations and are indicated appropriately. Figure 2 shows current transients from specimens that spent 0, 100, 200, and 300 s in the Pb-containing electrolyte prior to being transferred to the Pb-free electrolyte. The accelerating deposition in the Pb-containing electrolyte is shown at time less than zero. Deposition upon transfer to the Pb-free electrolyte was set at zero time for all specimens.

From Fig. 2, the longer the derivatization time in the Pb-containing electrolyte, the faster the subsequent Au deposition in the Pb-free electrolyte, consistent with higher coverage of the deposition rate-enhancing Pb adsorbate for longer derivatization time. The overall agreement just prior to transfer and just after decay of the insertion transient indicates that adsorbate coverage was generally not affected by the transfer step. Falling transients, consistent with consumption of the Pb adsorbate, are evident for derivatization periods of 200 and 300 s. Comparison to the current transients from
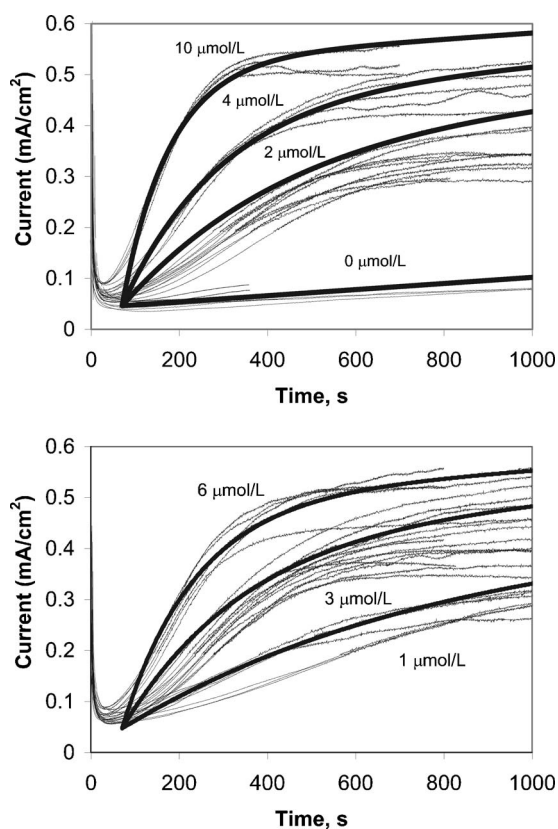
Figure 1. Current transients during Au deposition in electrolytes containing various concentrations of the $Pb(NO_3)_2$ additive (indicated) at a potential of -0.95 V SCE without agitation. The bold curves indicate the predicted behavior using the kinetics in Table I. Data is split to facilitate viewing.

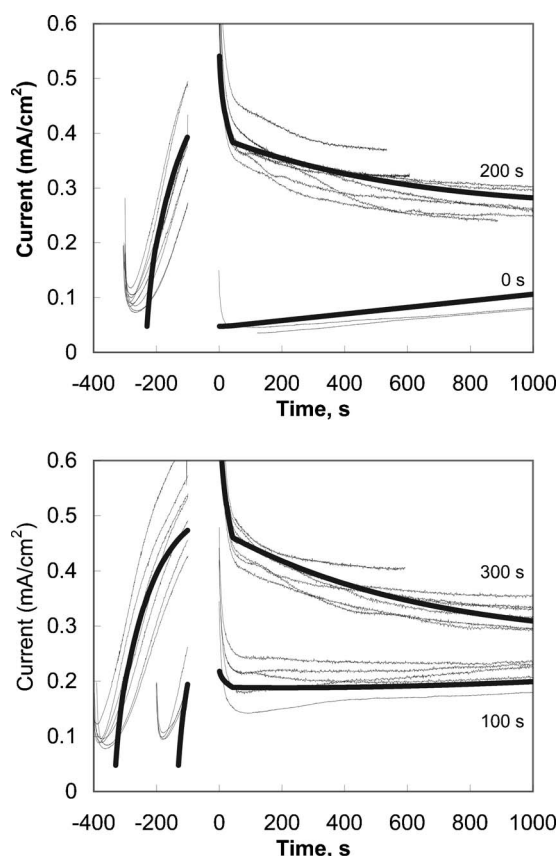**Figure 2.** Current transients from specimens with 0, 100, 200, and 300-s Au deposition in an electrolyte containing 10 μmol/L Pb followed by further Au deposition in a Pb-free electrolyte. The accumulation transients in the Pb-containing electrolyte, offset to allow comparison, are shown at times less than zero. Depositions upon transfer to the Pb-free electrolyte begin at zero time. Depositions were without agitation at a potential of -0.95 V SCE in both electrolytes. The bold curves indicate the predicted behavior using the kinetics in Table I. Data is split to facilitate viewing.

specimens without preadsorbed Pb (0 s derivatization) makes clear that the apparent increasing transient of the specimen derivatized for 100 s was dominated by the Pb-free baseline behavior.

The results of the current–decay transients, including those shown in Fig. 2, are summarized in Fig. 3 and 4. Figure 3 plots the average slope of each transient curve during the period between 100 and 300 s after transfer to the Pb-free electrolyte as a function of the average current density during the same period. This period was selected to minimize the impact of both initial specimen insertion transient and long-term surface roughening on the results. Figure 3 includes data for specimens derivatized in 10 μmol/L Pb-containing electrolyte, as in Fig. 2, and in 8 μmol/L Pb-containing electrolyte. Figure 4 plots the average current as a function of the derivatization time.

Assuming that the Au deposition current density scales with Pb coverage, Fig. 3 indicates the rate at which adsorbed Pb is consumed during Au deposition, presumably through incorporation, as an implicit function of the Pb coverage. Figure 4 is a measure of Pb adsorbate coverage on the surface of each specimen after it has been transferred from the Pb-containing electrolyte to the Pb-free electrolyte; consistently, the deposition rate (i.e., Pb adsorbate coverage) is seen to increase with derivatization time and at a faster rate in the higher concentration electrolyte.

Determining Kinetics from Studies on Planar Substrates

Kinetics for the feature filling simulations were obtained by fitting the predictions of Eq. 5 and 6 to the transient data in Fig. 1 and 2. In this fitting, $\kappa = 0$ in Eq. 6 because the specimens are planar. The predicted current–time transients for the data fitting were obtained by evolving the deposition rate and surface coverage according to Eq. 5 and 6 (with the initial adsorbate coverage θ_o and elec-

trolyte concentration C^o_{Pb} appropriate to the experiment) and simultaneously fitting the predictions to the rising transient data in Fig. 1 and the decaying transient data in Fig. 2. The required time-dependent interface concentration C^i_{Pb} required in Eq. 6 was obtained from the bulk electrolyte concentration by equating the rate of accumulation from the electrolyte onto the surface and the diffusive flux of Pb through the boundary layer

$$\Gamma k_+ C^i_{Pb}(1 - \theta) = \frac{D_{Pb}(C^o_{Pb} - C^i_{Pb})}{\delta} \qquad [7]$$

the left side of Eq. 7 being the Langmuir accumulation term in Eq. 6 multiplied by the areal density Γ of sites available on the surface for Pb adsorption. The value D_{Pb} in Table I has been equated to the diffusion coefficient of the $Au(CN)^-$ ion, D_{Au}, as previously used by other authors for Pb and Tl additives in similar electrolytes.[20,22] The steady-state boundary-layer thickness δ in Table I was obtained from the experimental limiting current density i_L using the expression

$$i_L = \frac{FD_{Au}C^o_{Au}}{\delta} \qquad [8]$$

with the values of the other parameters found in Table I.

Fit to the accumulation data.— Predicted rising transient behavior for the parameter values found in Table I and bulk catalyst concentrations $C^o_{Pb} = (0, 1, 2, 3, 4, 6,$ and $10)$ μmol/L are overlaid on the corresponding experimental data in Fig. 1. A 70-s time lag
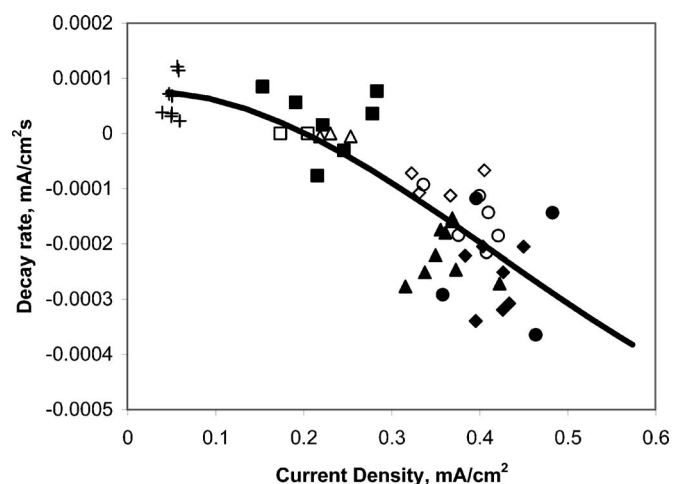
Figure 3. The average slopes of the decay transients during the period 100–300 s after transfer from the Pb-containing electrolyte to the Pb-free electrolyte is plotted as a function of the average deposition current during the same period. Data is included for specimens derivatized in 10 μmol/L Pb-containing electrolyte (closed symbols), as in Fig. 2, and 8 μmol/L Pb-containing electrolyte (open symbols). Derivatization times are indicated by: crosses (0 s), squares (100 s), triangles (200 s), diamonds (300 s), and circles (400+ s). A negative value indicates current density (deposition rate) decreases with time. The curve indicates the predicted behavior using the kinetics in Table I.

between immersion and the inception of accumulation/deposition was used to obtain better agreement between the predicted and experimental rising transient. This was necessary because no kinetic parameter adjustment was capable of yielding the gradually increasing deposition rates at the beginning of each rising transient (after the current drop upon specimen insertion). This gradual increase likely reflects the inception and initial evolution of the natural convection that underlies the boundary layer during deposition.[34] A 70-s time scale for development of the natural convection would be consistent with the time constant (δ^2/D_{Au}) required to develop the concentration gradient in the 270-μm-thick boundary layer. It is also reasonable considering the small density gradient that underlies the natural convection for deposition rates <0.5 mA/cm^2 and metal ion concentration of just 0.02 mol/L KAu(CN)$_2$. The predicted accumulation transients all include a constant current density drift to ac-
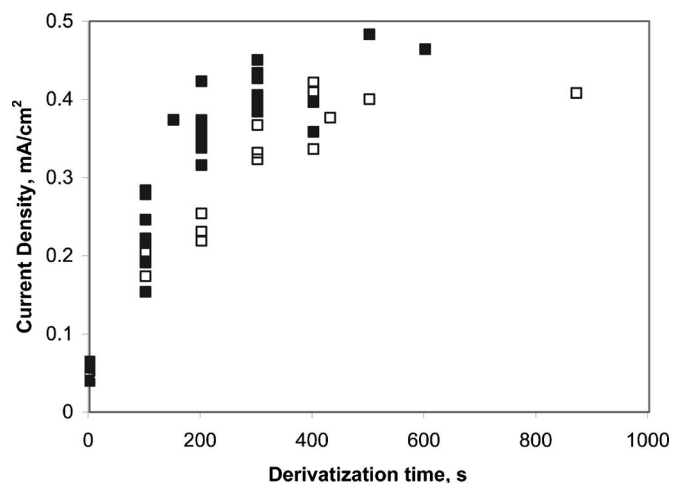

Figure 4. The average current during the period between 100 and 300 s after transfer to the Pb-free electrolyte was obtained from each curve in Fig. 4 and is plotted as a function of the derivatization time.

count for the increasing current noted earlier for deposition in the additive-free Au-cyanide electrolyte ($di/dt|_{drift} = 6 \times 10^{-5}$ mA/cm^2 s as per Table I and Fig. 2, 0 μmol/L case).

Fit to the consumption data.— Predicted transients for Pb accumulation followed by deposition in Pb-free electrolyte on the Pb-derivatized specimens are overlaid on the corresponding experimental data in Fig. 2. These predictions were obtained using the parameter values found in Table I, the accumulation portions, with $C_{Pb}^o = 10$ μmol/L, starting after the same 70-s time lag required to fit the accumulation curves in Fig. 1; as would be expected, the predicted accumulation curves are a poor fit to the experimental accumulation curves at early times. The decay portions of the curves were obtained using $C_{Pb}^o = 0$ μmol/L and initial Pb coverages θ_o = 0, 0.17, 0.512, and 0.7 for the accumulation times of 0, 100, 200, and 300s, respectively, equal to the final coverages from the predicted accumulation curves. In modeling the decay transients, the boundary-layer thickness δ used in Eq. 7 was presumed to initially thicken with the depleted zone, i.e., $\delta = \sqrt{D_{Au}t}$, until it reached the steady-state value given in Table I, after which time it was held constant. The concentration profile within the boundary layer was presumed to be fully relaxed throughout this evolution (i.e., a pseudo-steady-state approximation), and the predicted decay transients include the same constant current drift term noted earlier. Importantly, although the predicted transients are shown starting upon insertion, the kinetic parameters were obtained by fitting the data only beyond 100 s, consistent with the summarized data in Fig. 3, in order to avoid the uncetrtainty associated with the evolving convective and diffusion fields.

Comparison to the data in Fig. 3 was facilitated by derivation of a few equations. First, taking the time derivative of Eq. 5

$$\frac{di(\theta)}{dt} = (i^{\theta=1} - i^{\theta=0})\frac{d\theta}{dt}\left[1 + \frac{i^*(\theta)}{i_L}\right]^{-2} \quad [9]$$

which predicts the rate of current density change due to accumulation or consumption of the accelerating adsorbate. As noted previously, this was presumed to occur slowly enough that associated relaxation within the boundary layer could be assumed to be instantaneous. Equation 9 was modified by addition of the constant current drift term $di/dt|_{drift}$ noted earlier, which was presumed to also apply to the electrolytes containing the dilute Pb(NO$_3$)$_2$ additive

$$\frac{di(\theta)}{dt} = (i^{\theta=1} - i^{\theta=0})\frac{d\theta}{dt}\left[1 + \frac{i^*(\theta)}{i_L}\right]^{-2} + \frac{di}{dt}\bigg|_{drift} \quad [10]$$

The adsorbate evolution equation was expressed as a function of the adsorbate coverage θ alone by substitution of Eq. 5 into Eq. 6 (with $\kappa = 0$ and $C_{Pb}^o = 0$) to obtain

$$\frac{d\theta}{dt} = -k_-\theta\frac{\Omega_{Au}}{F}i^*(\theta)\left[1 + \frac{i^*(\theta)}{i_L}\right]^{-1} \quad [11]$$

Using Eq. 11, Eq. 10 was also expressed as a function of the adsorbate coverage θ alone

$$\frac{di}{dt} = -k_-\frac{\Omega_{Au}}{F}\theta i^*(\theta)(i^{\theta=1} - i^{\theta=0})\left[1 + \frac{i^*(\theta)}{i_L}\right]^{-3} + \frac{di}{dt}\bigg|_{drift}$$
$$[12]$$

With Eq. 11 and 12 both expressed as functions of θ, the predicted dependence of di/dt on i was readily evaluated using the parameters from Table I. The resulting curve is overlaid on the experimental data in Fig. 3.

The kinetic parameters $i^{\theta=0}$, $i^{\theta=1}$, k_+, and k_-, obtained from fitting the current transients in Fig. 1 and 2 and used to obtain all the predicted curves, are given in Table I.

Experimental Feature Filling

General Details.— Depositions on patterned substrates were accomplished in three steps. The first step involved deposition in agi-

Figure 6. Filling in a low-aspect-ratio trench on the same specimens shown in Fig. 5.
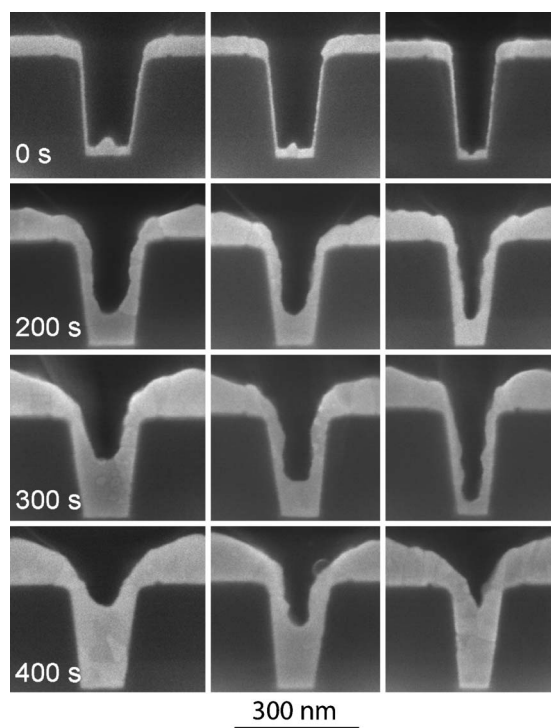
Figure 5. (top) Trenches with three different widths with only the evaporated Ti/Au seed. Filling of the same size trenches is shown after 100 s in the agitated Pb-free electrolyte, 60 s in the stagnant 10 μmol/L Pb derivatization electrolyte, and the indicated deposition times in the agitated Pb-free electrolyte. All depositions were at −0.95 V SCE.

tated Pb-free electrolyte at −0.95 V SCE. This step was primarily used to ensure that a good seed existed for the superfill process. The second step involved derivatization in stagnant Au-cyanide electrolyte containing 10 μmol/L $Pb(NO_3)_2$ for adsorption of the Pb accelerator, concurrent with Au deposition, at −0.95 V SCE. The final step involved the majority of the Au deposition and was conducted in agitated Pb-free electrolyte at −0.95 V SCE. All immersions were done at potential, and transfers between solutions were done as quickly as possible to try to ensure that the specimens remained wetted with the relevant electrolyte during the transfers; the elapsed time between the emmersion starting and immersion ending each transfer was nonetheless ~30 s due to the need to transfer beakers, shift electrode connections, and adjust specimen position. Efforts were also made to minimize carryover to the frequently refreshed, additive-free solution.

The separation of the Pb derivatization and Au deposition between the second and third steps, respectively, though not complete because there was concurrent Au deposition during the second step, permitted agitation to reduce Au ion depletion during feature filling without affecting the kinetics of the Pb adsorption process. In contrast, industrial processes for Cu superfill typically conduct the entire deposition in a single electrolyte containing both metal ions and additives. Deposition on specimens with preadsorbed accelerator and zero accelerator concentration in the electrolyte has been previously demonstrated to yield CEAC-quantifiable superfill during both Cu and Ag electrodeposition[12,15,35] that is indistinguishable from superfill obtained through single electrolyte processes.

Experimental results.— Figure 5 shows sequential filling of three trenches of different width, all approximately 0.2 μm deep. Figure 6 shows sequential filling of a much wider trench. All images with identical processing parameters come from the same specimen, as each specimen included arrays of all the trench widths studied. The derivatization time in the 10 μmol/L $Pb(NO_3)_2$-containing
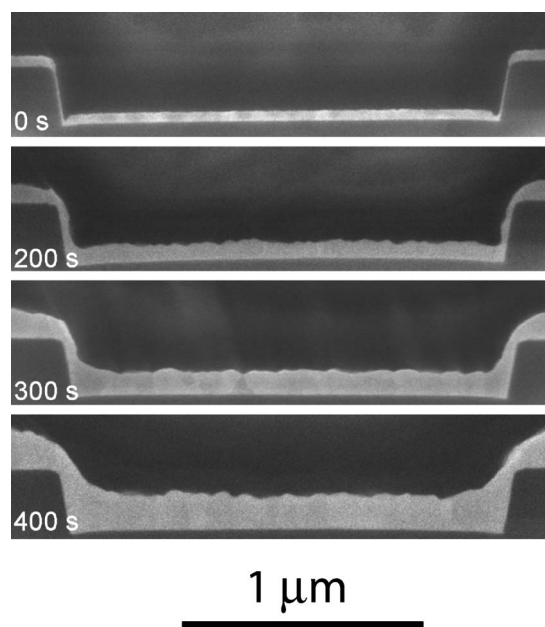
electrolyte was 60 s for all three plated specimens; the subsequent deposition time in the Pb-free electrolyte ranged from 200 to 400 s. The bottom-up filling associated with the superfill process is particularly visible in the two wider trenches of Fig. 5. The enhanced deposition at the corners of the very wide trench in Fig. 6 is also a manifestation of superfilling. Details concerning the process for cross-section preparation can be found in a previous publication.[4]

Figure 7 shows the currents recorded during filling of the patterned specimens shown in Fig. 5 and 6; the current history for each specimen has been normalized by the steady-state current at the end of its initial Pb-free deposition step (from 0 to 100 s). The initial deposition in the Pb-free electrolyte exhibits a gradual decay to steady state for each Pb-free surface. The decay is likely related to evolution of the boundary layer and associated gold complexes. Accumulation of Pb adsorbate during the 60-s derivatization step (between approximately 140 and 200 s on Fig. 7) manifests as the rising transient after the decay of the insertion transient. The final Au depositions exhibit a gradually rising current from a value that is approximately four times larger than the value on the Pb-free sur-
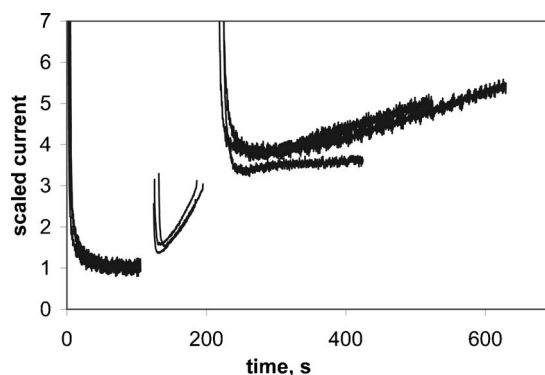

Figure 7. The recorded deposition currents for the three specimens pictured in Fig. 5 and 6, normalized by the steady-state current from the first deposition step in the Pb-free electrolyte.
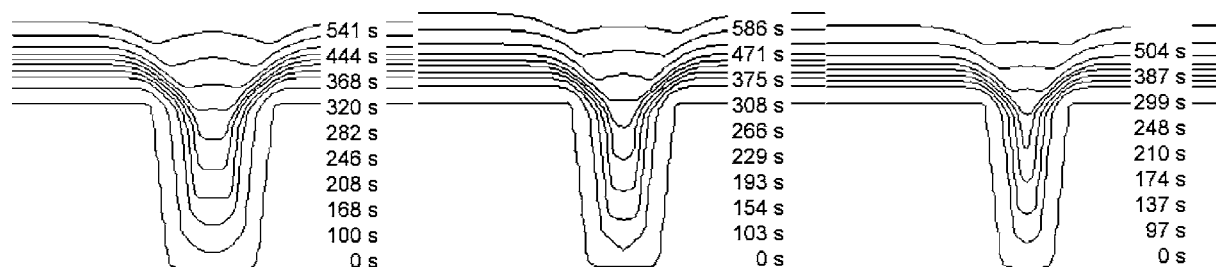
Figure 8. Simulations of deposition in trenches with preadsorbed Pb coverage $\theta_o = 0.15$ during Au deposition in agitated Pb-free electrolyte. Deposition is shown in trenches with dimensions from Table II, corresponding to the experimental filling in Fig. 6.

face. The gradual increase of current during this last step is likely due to increasing surface area (Fig. 5: note the curvature of the surface between trenches after 400-s deposition).

Superfill Modeling Using the CEAC Mechanism

CEAC-based feature-filling predictions were made as follows. The first equality in Eq. 4 expressed the local current density (and thus deposition rate) in terms of the local Au ion concentration and Pb coverage θ. Equation 6 defined the local evolution of the adsorbate coverage θ in terms of the local deposition rate. Required kinetics were from Table I, as obtained from the studies on planar substrates. Transport of the Au ions through the boundary layer in the agitated electrolyte and within the unfilled region of the trench was presumed to be through diffusion, satisfying the fully time-dependent diffusion equation and mass conservation boundary conditions on the surface of the growing Au deposit for a periodic array of trenches. Geometrical parameters defining the trenches, including width at the trench bottom, trench pitch (center-to-center spacing), and sidewall tilt angle were obtained from the imaged trenches (see Fig. 5) as listed in Table II. A nearly threefold increase of measured limiting current density in the agitated electrolyte (not shown) was modeled as a reduced boundary layer thickness, as indicated in Table I.

Estimating initial adsorbate coverage.— The experimental filling results in Fig. 5 and 6 could be modeled numerically by dividing the deposition process into its three steps and simulating each one in sequence. However, the offset of the fitted transients to the experimental accumulation data in Fig. 1, where the accumulation of adsorbate starts only after 70 s, precluded meaningful use of Eq. 6 for assessing adsorbate coverage at the 60-s derivatization time used for the specimens shown in Fig. 5 and 6.

Instead, the final adsorbate coverage at the end of the derivatization step, θ_o, was extracted from the measured increase of the deposition current from deposition step 1 to step 3 induced by the Pb adsorption step (see Fig. 7). Filling during the third step was then simulated with this starting coverage θ_o. Deposition during the unaccelerated, first step and relatively short, still-accelerating derivatization step was ignored. Neglect of the deposition associated with the first two steps is a reasonable approximation considering the

deposit thickness after an additional 200 s of deposition on the accelerated surface (compare the top two rows of either Fig. 5 or Fig. 6).

For the transients shown in Fig. 7 in particular, the deposition current increased by a factor of approximately 4 as result of the derivatization (ignoring the insertion transients). Using Eq. 1 with the parameters in Table I, this corresponds to increasing the Pb adsorbate coverage to approximately $\theta_o \approx 0.14$ [i.e., predicted current density going from $i(0) \approx 0.05$ mA/cm^2 to $i(0.14) \sim 0.2$ mA/cm^2, ignoring Au-ion depletion which is difficult to assess accurately because of the large variations in trench width and pitch across the surfaces of the patterned specimens].

Feature fill simulations.— Figure 8 shows simulations obtained for deposition in derivatized trenches during Au deposition in the Pb-free electrolyte. The trench dimensions and simulation conditions correspond to those of the experimental images in Fig. 5 and 6, using the kinetics from Table I, geometries from Table II, and initial Pb coverage of $\theta_o = 0.15$. The general formalism of the numerical evaluation can be found in Ref. 11. The specific code used for the numerical simulation is publicly available.[36]

Table II. Geometrical parameters for fill modeling as obtained from patterned specimens.

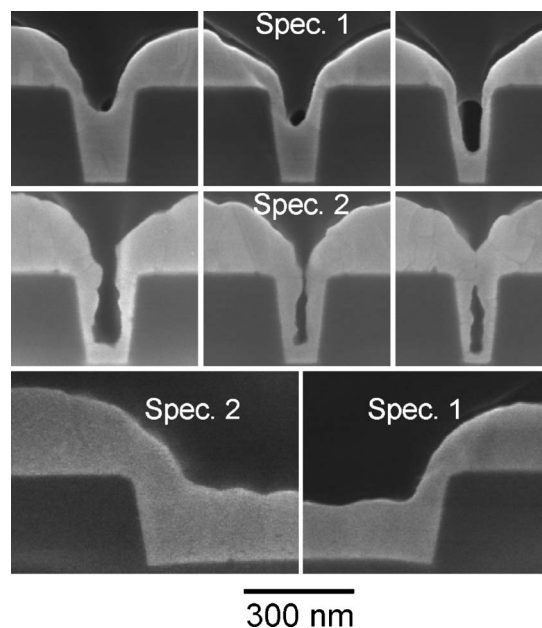|	
Height, μm	0.2
Sidewall tilt, degrees	6
a. Width at bottom, μm	0.115
a. Pitch, μm	0.6
b. Width at bottom, μm	0.095
b. Pitch, μm	0.55
c. Width at bottom, μm	0.07
c. Pitch, μm	0.5

Figure 9. Filling in two nominally identical specimens. Filling of the same size trenches as shown in Fig. 5 as well as one end of the wide trench pictured in Fig. 6. Deposition for 100 s in the agitated Pb-free electrolyte, 180 s in the stagnant 10 μmol/L Pb derivatization electrolyte, and 400 s in the agitated Pb-free electrolyte. All depositions were at -0.95 V SCE.
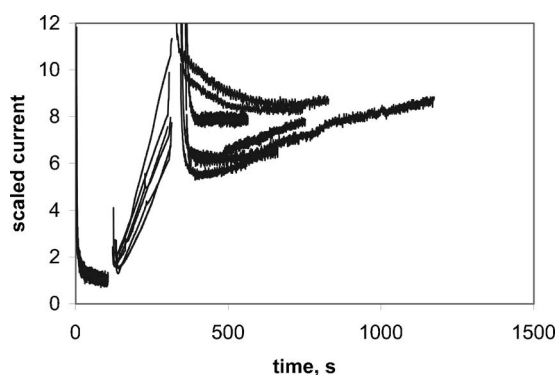
Figure 10. The recorded deposition currents for specimens derivatized for 180 s, including the two specimens pictured in Fig. 8. The currents are normalized by the steady-state currents recorded during the first deposition step in the Pb-free electrolyte.

Comparison to experiment.— The CEAC model predictions in Fig. 8 capture the geometry of superfill in the wide trench in Fig. 5, though the fill time is somewhat underestimated. The predictions also capture the experimentally observed transition from bottom-up filling to v-notch that accompanies decrease of the trench width (Fig. 5, 400-s deposition). While fill time is predicted to decrease somewhat with decreasing trench width, experimental filling of the wider trench is clearly faster than that of the intermediate trench. This result is quite interesting in that it contrasts with both copper and silver superfill, which exhibit the predicted increase of fill time with feature width.[12,15]

Discussion

There was significant variability of the experimental Au fill results. Specifically, runs with nominally identical processing, i.e., derivatization time and deposition time, exhibited varying degrees of feature filling. Examples of two specimens with substantially different filling in spite of nominally identical processing, 180-s derivatization and 400-s final deposition, are shown in Fig. 9. The origin of some of the variability in filling can be understood from the corresponding current transients in Fig. 10, which shows all the transients from specimens that were derivatized for 180 s. Specimen 2 with its thick, voided deposits yielded the uppermost (decaying) current transient after the derivatization (scaled current ~ 11, corresponding to $\theta_o \approx 0.46$, ignoring Au-ion depletion). The only other specimen to exhibit voiding (not shown) yielded the other gradually decaying transient, with its high scaled current (~ 10). In contrast, specimen 1 of Fig. 9, with its bottom-up filling, yielded one of the lower clusters of rising curves (scaled current ~ 6, corresponding to $\theta_o \approx 0.23$, ignoring Au-ion depletion).

Figure 11 shows simulations using a starting coverage of $\theta_o = 0.45$ (as per the uppermost current transient in Fig. 10 and corresponding to specimen 2 of Fig. 9). The superfill dynamic is predicted to occur only for the widest trench, with deep v-notch cusps of conformal filling predicted for the two other trenches; seam formation is avoided only because the tilted sidewalls permit geometrical leveling to fill the trench. This shift toward conformal fill-

ing is understood to occur because the initially high adsorbate coverage precludes significant acceleration of local deposition through the CEAC mechanism.

The corresponding experimental filling (specimen 2 of Fig. 9) has in fact lost the bottom-up filling dynamic, as predicted. However, superfill of all three trench widths has been lost rather than just the predicted two, and voiding is observed rather than the predicted v-notch, conformal filling. Deposition within the features is also slower than predicted, particularly in comparison to that in the field. These observations suggest substantial metal ion or adsorbate depletion within the trench. However, the Au-ion depletion within the feature was accounted for in these simulations, and other simulations (not shown) indicated minimal depletion of accelerator would be expected to occur during the Pb derivatization step.

Nonideal aspects of superfill.— Several nonideal aspects of superfill in this system might underlie the tendency of the model to overestimate deposition rates as well as the difference between predicted and observed dependence of fill time on trench width.

Free cyanide concentration.— If the same kinetics apply, the CN that is rejected from the interface during the Au deposition would be expected to induce a gradient of opposite sign and of twice the magnitude of that of the arriving Au-cyanide ion [two CN for each Au in the $Au(CN)_2^-$]. For transport-limited deposition this could increase the free-cyanide concentration adjacent to the surface by as much as 40% (from 0.1 mol/L to 0.14 mol/L given the 0.1 mol/L KCN and 0.02 mol/L $KAu(CN)_2$ concentrations). Such an increase would be expected to shift the potential for local equilibrium such that further Au deposition would be retarded. This would be expected to be more significant in regions of higher areal density and in narrower features and would be consistent with the observed decrease of deposition rate with decreasing trench width (and pitch) visible in Fig. 5 and Fig. 9 (specimen 1). Simulations including this effect would require data on the impact of cyanide concentration on the Pb-accelerated Au deposition rate. This task, going beyond the scope of the envisioned CEAC-based modeling effort, has been left for the future.

Adsorbate consumption.— The simulations capture the impact of area change, accumulation, and consumption on adsorbate coverage and feature filling through Eq. 6. The consumption term, which quantifies the failure of the adsorbate to remain on the surface, is a deviation of the actual system from the ideal CEAC mechanism of superfill. For the parameters in Table I, the consumption term yields exponential decay of the preadsorbed Pb coverage by a factor of 1/e after deposition of $1/k_- \approx 0.3$ μm Au. As the trenches used for experimental superfill were significantly narrower than this value, predicted consumption of adsorbate on the sidewalls during deposition on these surfaces was fairly small. For conditions where superfill did occur, coverage on the upward-moving bottom surface was predicted to be dominated by the area change term, as the adsorbate from the eliminated sidewall area all ended up on this surface. Thus, the consumption term was predicted to have played only a small role in the observed filling and is not believed to underlie the observed differences between prediction and experiment. Using values from Table I, the Pb incorporation, equal to $k_-\Gamma\theta$ and maximum at $\theta = 1$, is less than 2×10^{-5} mol/cm^3, or, using the 7.11 cm^3 molar volume of Cu, less than 3×10^{-6} atomic fraction.
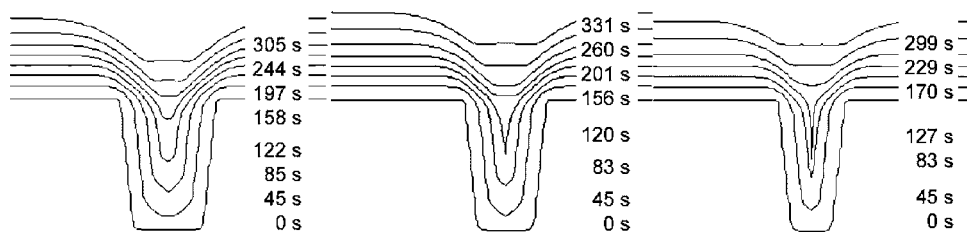

Figure 11. Simulations of trench filling for preadsorbed Pb coverages of θ_o = 0.45 filling in the Pb-free electrolyte. Kinetics used for the simulations can be found in Table I. Trench dimensions and pitches used for the modeling are given in Table II.

Surface diffusion.— Surface diffusion of the adsorbed accelerator, by reducing spatial gradients of adsorbate coverage, works against the CEAC-induced variations that underlie the superfill mechanism. Surface diffusion was neglected in this study, as in previous CEAC models. The presence of sharp corners on the growth contours in Cu superfill, in full agreement with CEAC predictions, supports neglect of surface diffusion in that system. In contrast, the rounding of the filling contours in Fig. 5, as opposed to the sharp corners of the corresponding CEAC predictions, suggests that surface diffusion of the Pb adsorbate might be more significant in the system studied here. This is not unreasonable given that the depositions times are approximately 2 orders of magnitude longer than those typical of Cu superfill. Nonetheless, while surface diffusion would be expected to be most detrimental to filling of the smallest trenches, consistent with observation, it would not be expected to retard deposition rates within the trenches, as suggested by the pinch-off voids in Fig. 9 specimen 2, nor does it seem likely that it would vary substantially over the small range of dimensions studied here. Modeling of the impact of surface diffusion of the catalyst on feature superfill is left for the future.

Phase formation.— Lead and gold form several intermetallic phases. While the consumption rate experiments detailed in Fig. 2 indicate the adsorbed lead generally segregates to the surface at the coverages studied, it is possible that such phase formation could spontaneously occur at sufficiently high fractions θ of the saturation coverage Γ used. As the location with highest θ is generally the upward-moving bottom surface, with its CEAC-enhanced coverage, such phase formation, if associated with increased consumption, would be expected to negatively impact superfill. In the absence of data to the contrary, consumption of the Pb adsorbate has been modeled using the kinetics obtained from modeling of the transient data in Fig. 1 and 2.

Conclusions

Bottom-up superfill of gold in trenches with a preadsorbed sub-monolayer coverage of Pb was explored quantitatively. The impact of Pb adsorption from the electrolyte on the rate of Au deposition and the kinetics of the Pb consumption process were explored through studies on planar substrates. The obtained kinetics were then used in the CEAC mechanism of superfill to quantitatively predict Au superfill in trenches with submicrometer dimensions. Agreement of prediction with experimental filling geometry was good for the trenches studied, including bottom-up fill geometry and transition from superfill to v-notch filling with decreasing trench width. In contrast to prediction, however, filling rates decreased with trench width and voiding rather than seam formation occurred at the highest adsorbate coverages. Thus, while this work presented the first quantitative prediction of Au superfill, it also signals the need for further study.

References

1. P. C. Andricacos, C. Uzoh, J. O. Dukovic, J. Horkans, and H. Deligianni, *IBM J. Res. Dev.*, **42**, 567 (1998).
2. A. V. Davydov, L. A. Bendersky, W. J. Boettinger, D. Josell, M. D. Vaudin, K. S. Chang, and I. Takeuchi, *Appl. Surf. Sci.*, **223**, 24 (2004).
3. T. J. Kim and P. H. Holloway, *Crit. Rev. Solid State Mater. Sci.*, **22**, 239 (1997).
4. D. Josell, C. R. Beauchamp, D. R. Kelley, C. A. Witt, and T. P. Moffat, *Electrochem. Solid-State Lett.*, **8**, C54 (2005).
5. Z. Hu and T. Ritzdorf, Abstract 147, The Electrochemical Society Meeting Abstracts, Vol. 2004-1, San Antonio, TX, May 9–13, 2004.
6. Y. Cao, P. Taephaisitphongse, R. Chalupa, and A. C. West, *J. Electrochem. Soc.*, **148**, C466 (2001).
7. A. C. West, S. Mayer, and J. Reid, *Electrochem. Solid-State Lett.*, **4**, C50 (2001).
8. D. Josell, D. Wheeler, W. H. Huber, and T. P. Moffat, *Phys. Rev. Lett.*, **87**, 016102 (2001).
9. T. P. Moffat, D. Wheeler, W. H. Huber, and D. Josell, *Electrochem. Solid-State Lett.*, **4**, C26 (2001).
10. D. Josell, D. Wheeler, W. H. Huber, J. E. Bonevich, and T. P. Moffat, *J. Electrochem. Soc.*, **148**, C767 (2001).
11. D. Wheeler, D. Josell, and T. P. Moffat, *J. Electrochem. Soc.*, **150**, C302 (2003).
12. T. P. Moffat, D. Wheeler, M. Edelstein, and D. Josell, *IBM J. Res. Dev.*, **49**, 19 (2005).
13. T. P. Moffat, B. Baker, D. Wheeler, J. E. Bonevich, M. Edelstein, D. R. Kelly, L. Gan, G. R. Stafford, P. J. Chen, W. F. Egelhoff, and D. Josell, *J. Electrochem. Soc.*, **149**, C423 (2002).
14. D. Josell, B. Baker, C. Witt, D. Wheeler, and T. P. Moffat, *J. Electrochem. Soc.*, **149**, C637 (2002).
15. B. C. Baker, C. Witt, D. Wheeler, D. Josell, and T. P. Moffat, *Electrochem. Solid-State Lett.*, **6**, C67 (2003).
16. B. C. Baker, M. Freeman, B. Melnick, D. Wheeler, D. Josell, and T. P. Moffat, *J. Electrochem. Soc.*, **150**, C61 (2003).
17. D. Josell, S. Kim, D. Wheeler, T. P. Moffat, and S. G. Pyo, *J. Electrochem. Soc.*, **150**, C368 (2003).
18. R. Yu. Bek, *Russ. J. Electrochem.*, **38**, 1237 (2002).
19. R. Yu. Bek and L. I. Shuraeva, *Russ. J. Electrochem.*, **39**, 229 (2003).
20. R. Yu. Bek and L. I. Shuraeva, *Russ. J. Electrochem.*, **39**, 872 (2003).
21. B. Bozzini and A. Fanigliulo, *J. Cryst. Growth*, **243**, 190 (2002).
22. J. D. E. McIntyre and W. F. Peck, Jr., *J. Electrochem. Soc.*, **123**, 1800 (1976).
23. Dj. Davidović and R. R. Adzić, *Electrochim. Acta*, **33**, 103 (1988).
24. P. Bindra, D. Light, P. Freudenthal, and D. Smith, *J. Electrochem. Soc.*, **136**, 3616 (1989).
25. D. Poškus, G. Agafonavas, and I. Jurgaitiene, *J. Electroanal. Chem.*, **425**, 107 (1997).
26. E. T. Eisenmann, *J. Electrochem. Soc.*, **125**, 717 (1978).
27. S. Nakahara and Y. Okinaka, *J. Electrochem. Soc.*, **128**, 284 (1981).
28. T. Sawaguchi, T. Yamada, Y. Okinaka, and K. Itaya, *J. Phys. Chem.*, **99**, 14149 (1995).
29. F. Huerta, C. Mele, B. Bozzini, and E. Morallon, *J. Electroanal. Chem.*, **569**, 53 (2004), And references therein.
30. Y. Okinaka and M. Hoshino, *Gold Bull.*, **31**, 3 (1998).
31. D. Davidović and R. R. Adžić, *J. Serb. Chem. Soc.*, **53**, 499 (1988).
32. R. R. Adzic, in *Advances in Electrochemistry and Electrochemical Engineering*, Vol. 13, H. Gerischer and C. W. Tobias, Editors, J. Wiley and Sons, New York (1994).
33. D. Roha and U. Landau, *J. Electrochem. Soc.*, **137**, 824 (1990).
34. J. S. Newman, *Electrochemical Systems*, 2nd ed., p. 363, Prentice-Hall, Englewood Cliffs, NJ (1991).
35. T. P. Moffat, D. Wheeler, C. Witt, and D. Josell, *Electrochem. Solid-State Lett.*, **5**, C110 (2002).
36. D. Wheeler, J. Guyer, and J. A. Warren, "FiPy: A Finite Volume PDE Solver Using Python" at http://www.ctcms.nist.gov/fipy